ELSEVIER

Journal of Loss Prevention in the Process Industries 14 (2001) 269–282

Journal of Loss Prevention in the process industries

www.elsevier.com/locate/jlp

The influence of injector design on the decay of pre-ignition turbulence in a spherical explosion chamber☆

David B. Mercer [a], Paul R. Amyotte [a], Debbie J. Dupuis [b], Michael J. Pegg [a,*], Arief Dahoe [c], Wouter B.C. de Heij [c], John F. Zevenbergen [c], Brian Scarlett [c]

[a] *Department of Chemical Engineering, Dalhousie University, PO Box 1000, Halifax, Nova Scotia, Canada, B3J 2X4*
[b] *Department of Engineering Mathematics, Dalhousie University, PO Box 1000, Halifax, Nova Scotia, Canada, B3J 2X4*
[c] *Division of Particle Technology, Delft University of Technology, Delft, The Netherlands*

Abstract

This paper reports on an experimental study to characterize the turbulent flow field inside a 20 l Siwek chamber during the pre-ignition period. An acrylonitrile–butadiene–styrene model of the chamber was constructed with optical quality windows enabling laser Doppler anemometry (LDA) to be used for turbulence measurements. Alumina (Al_2O_3) particles were used as the seed dust for measuring the gas-phase turbulence. Three specific dust dispersion systems have been investigated: (1) the deflector plate (also referred to as the rebound nozzle); (2) the perforated annular nozzle; and (3) the circular "Dahoe" nozzle. It is assumed that changing the method of dust dispersion alters the turbulence characteristics. The flow field is non-stationary, i.e., the mean (or predominant fluid flow) and superimposed velocity fluctuations upon the mean decrease with time. Furthermore, there are variations from injection to injection. A procedure has been developed to analyze this non-stationary signal to extract the mean and fluctuating components of velocity, thereby paving the way for decay "laws" to be determined for a particular nozzle configuration.

Keywords: Dust explosion testing; Turbulence; Turbulent decay

1. Introduction

Dust explosions are a major hazard in many industrial processes. In operations such as crushing and grinding, conveying, classifying and storage, an explosion may occur in the presence of combustible dusts or powders. Such explosions can result in loss of production, process equipment and quite possibly human life. The British Materials Handling Board (BMHB) identified a broad range of industrial equipment involved in dust explosions throughout the United Kingdom. The BMHB analysis of dust explosions and fires (Abbott, 1985) cited 143 incidents during the years 1979–1984. A further analysis by Porter (1989), based on data from the United Kingdom Health and Safety Executive, cited 160 incidents. Mills, dryers and filters were involved in the largest percentage of these 303 incidents. Jeske and Beck (1989) compiled an informative overview of dust explosions in the Federal Republic of Germany covering the years 1965–1985 and included a total of 426 dust explosions. In a recent study, Kauffman, Mestrich, Regan, and Seymour (1996) presented information on dust explosions in the US grain industry covering the years 1985–1994. In comparing fire and explosion data from the UK, Germany and the USA, silos/storage systems, milling operations and dust collection systems rank high amongst processing equipment where dust explosions occur. Other plant equipment, such as mixers, rank low based on their history of incidents. Nevertheless, dust explosions remain a persistent threat to process equipment and human life. Although safer plant operation has been made possible by the identification of the need for good housekeeping, removal of ignition sources, sensible location of physical plant, admixture of inerts to hazardous materials, and venting of enclosures, the need for further research does exist.

To adequately protect plant-processing equipment, it

☆ Based on a paper presented at the 8th International Colloquium on Dust Explosions, Schaumburg, IL, USA, 21–25 September 1998.

* Corresponding author. Address for correspondence: Department of Petroleum and Minerals Resources Engineering, Sultan Qaboos University, PO Box 33, Al-Khod 123, Muscat, Sultanate of Oman.
E-mail address: peggm@squ.edu.om (M.J. Pegg).

0950-4230/01/$ - see front matter
PII: S0950-4230(00)00051-6

is important to know both the maximum overpressure and the maximum rate of pressure rise to be expected should a dust explosion occur. To measure these parameters, various laboratory-scale tests have been developed over the past 120 years. A summary of current closed-vessel test methods to assess dust explosion parameters is presented in Table 1.

The common thread between closed-vessel testing outlined in Table 1 is the fact that a blast of compressed air is used to disperse the test dust inside the main vessel, thereby producing a dust/air suspension prior to ignition. Clearly, dispersion is an essential prerequisite for a dust explosion. The blast of compressed air also generates turbulence within the dust/air suspension. Furthermore, since a blast of air is used to disperse the dust instead of a continuous flow, the degree of turbulence inside the test vessel decays once the injection of air stops. The ignition delay time, therefore, determines the degree of turbulence in the dust cloud at the moment of ignition. Longer ignition delay times result in a lower degree of pre-ignition turbulence and thereby a lower value of $K_{St}=(dP/dt)_{max}V^{1/3}$ (i.e., maximum rate of pressure rise, normalized by the cube root of the vessel volume). This effect is shown in Fig. 1 taken from the work of van der Wel, van Veen, Lemkowitz, Scarlett, and van Wingerden (1992) for lycopodium dust in a 20 l chamber. At high levels of turbulence, the effective flame front area is distorted resulting in rapid propagation with explosion violence reaching high values. Since the degree of pre-ignition turbulence has a significant effect on K_{St}, the level of turbulence can also strongly affect venting requirements. As the degree of turbulence increases, so does the combustion rate and the rate of pressure rise, which results in a greater area required to successfully vent the volume of gases produced by the explosion (Lunn, 1992).

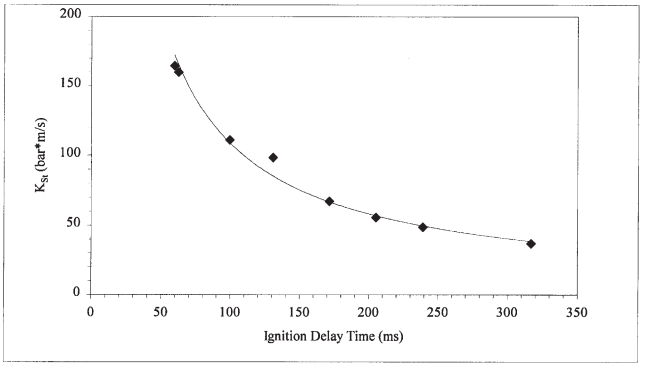

Fig. 1. K_{St} versus ignition delay time for a 500 g/m^3 suspension of lycopodium. From van der Wel et al. (1992).

With reference to Table 1, for dust explosion testing in the standard International Standards Organization (ISO) 1 m^3 vessel, an ignition delay time of 600 ms has been selected. This value is only valid if a 5 l air storage canister is used. If the ignition delay time is changed, pre-ignition turbulence levels will vary, resulting in different values of K_{St}. If low-density dusts are used it may be necessary to use a 10 l air storage canister. In this case, the ignition delay time (degree of pre-ignition turbulence) must be altered so results obtained with the 10 l air storage canister replicate those obtained with the 5 l canister. Inspection of Fig. 2, taken from Bartknecht (1989), shows that a 10 l canister produces a higher degree of turbulence than a 5 l cannister, resulting in significantly different values of K_{St}. Thus, for dust testing in the standard ISO 1 m^3 vessel using a 10 l air storage canister, the ignition delay time must be changed to 900 ms to obtain comparable results with the 5 l storage canister (Lunn, 1992).

In Siwek's quest to develop a laboratory-scale apparatus able to reproduce results that matched the larger

Table 1
Summary of current closed-vessel test methods

	Siwek 20 l apparatus	ISO 1 m^3 Chamber
Reference	ASTM E1226-94 (1994)	ISO 6184/1 (1985)
Vessel volume (l)	20	1000
Vessel geometry	Spherical	Cylindrical
Length/diameter ratio	1/1	1/1
Nominal surface area/volume ratio (m^2/m^3)	18/1	5/1
Vessel pressure before initiation of test [bar absolute]	0.40	1.0
Number of air storage canisters	1	1
Air storage canister volume (l)	0.6	5.0
Air storage canister pressure before initiation of test [bar absolute]	21.0	21.0
Placement of dust: directly in vessel or in air storage canister	Air storage canister	Air storage canister
Type of dust dispersion system(s)	1. Perforated annular nozzle 2. Rebound nozzle	Perforated semi-circular spray pipe
Nozzle geometry: number of holes, hole diameter (mm)	1. 112 holes of 3 mm ∅ 2. Plate-type deflector nozzle	16 holes, of 5 mm ∅
Ignition source	Pyrotechnic igniters	Pyrotechnic igniters
Ignition source strength (J)	2×5000	2×5000
Ignition delay time (ms)	60	600

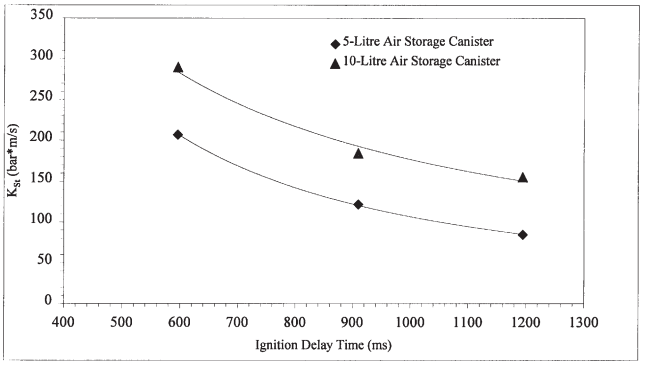

Fig. 2. K_{St} versus ignition delay time for a suspension of cellulose dust in an ISO 1 m^3 vessel with an ignition energy of 10 kJ. From Bartknecht (1989).

ISO 1 m^3 vessel, about 10,000 closed-vessel tests were conducted (Siwek, 1980). In this systematic series of experiments, laboratory vessels of different geometries and volumes were used. Also, three different dispersion nozzles were evaluated in an attempt to produce results in accordance with the cube-root scaling relationship. His results showed that when the dust dispersion system was changed in the sequence mushroom nozzle→ball nozzle→ring nozzle, the measured explosion indices approached those measured in the ISO 1 m^3 vessel. Siwek determined that 17 l was the minimum spherical volume needed to generate results comparable to the ISO 1 m^3 vessel, and so a 20 l test chamber was constructed (Siwek, 1980). However, when using the new 20 l vessel in combination with the dust dispersion system from the previous 10 l sphere, measured maximum rates of pressure rise still did not obey the cube-root scaling relationship. After several attempts at modifying the dust dispersion system, the final perforated annular nozzle design produced results that scaled to those of the ISO 1 m^3 vessel. It is obvious that any deviation from the standard operating procedures of current-day dust explosion test vessels, such as changes in the volume of the air storage canister, ignition delay time, dust dispersion system, the vessel geometry or size, will strongly influence the resulting explosion parameters, especially the K_{St} value. The results of such changes can be so drastic that even if the standard ignition delay time is used, there will be no correlation with results obtained from the standard ISO 1 m^3 vessel. This in turn can lead to gross overdimensioning or underdesign of plant-sized equipment, both having significant financial consequences. Clearly, any adjustment in the above-mentioned parameters is merely an exercise in manipulating the pre-ignition turbulence inside the test vessel to produce the desired results. In view of pre-ignition turbulence strongly influencing explosion parameters (especially the K_{St} value), the influence of turbulence on explosion development is the primary area of emphasis of this work. Therefore, the main objective of the present study was to characterize the turbulent flow field developed inside the 20 l chamber during the air dispersion process.

2. Previous studies

A review of recent literature has identified four research groups who have attempted to measure the influence of turbulence on closed-vessel dust explosions. These groups have placed particular emphasis on investigations in spherical or nearly spherical vessels. In all cases, the investigations were conducted in apparatus used for standard American Society for Testing and Materials (ASTM) or ISO test methods. A summary of the literature is presented in Table 2.

Pu, Jarosinski, Johnson, and Kauffman (1990) measured turbulence parameters inside a 20 l Siwek chamber using the perforated annular nozzle and various air storage canister pressures; namely 10, 20 and 30 bar gauge. Results of instantaneous velocity, root-mean-square (RMS) turbulent velocity and integral length scale were presented as a function of time. Measurements were made using hot wire anemometry (HWA), with the probe located in the center of the vessel, while injecting dust-free air. Their results indicated that the dispersion process in the 20 l Siwek chamber is highly time-dependent, and somewhat dependent upon air storage canister pressure. It was determined that instantaneous velocities reach maximum values of about 10–13 m/s, then decay rapidly to approximately 0 m/s after 400 ms. Likewise, RMS turbulent velocities showed similar behavior. Maximum RMS turbulent velocities of about 3 m/s were calculated and these decayed to about 1.5 m/s in 100 ms, 0.5 m/s in 200 ms, and finally to around 0.25 m/s in 400 ms. The RMS velocity is defined as (Bradshaw, 1971):

$$U_{\mathrm{RMS}} = \sqrt{\overline{(U')^2}}, \tag{1}$$

where U' is the superimposed fluctuation on the mean flow. The overbar denotes an average quantity. To compute U_{RMS} for a non-stationary flow requires selecting an "appropriate" time window over which to average the signal. This approach assumes that the "turbulence" can be considered stationary within the selected time window. Implicit in this approach is that the time window is less than any characteristic turbulent time scale of the actual non-stationary flow. Furthermore, it is usual to ensemble average over many runs. Pu et al. (1990) used data from eight to 15 runs but unfortunately provided no information on selection of a time window from which to calculate U_{RMS}. A further problem with their measurement technique (as acknowledged by them) was that HWA is directionally insensitive. Effectively this means they measured the speed of the flow (i.e., the magnitude but not the direction).

Table 2
Turbulence investigations in spherical or nearly spherical closed-vessel apparatus, 1990–present

Researchers	Vessel	Dust dispersion system	Air volume (l)	Air pressure [bar(g)]	Measurement technique	Measured characteristics
Pu et al. (1990)	Siwek 20 l apparatus	Perforated annular nozzle	0.6	10 20 30	Hot wire anemometry (HWA)	• Instantaneous velocities • RMS turbulent velocities • Integral length scale
van der Wel et al. (1992)	Siwek 20 l apparatus	Perforated annular nozzle	0.6	20	HWA	• RMS turbulent velocities
	ISO 1 m^3 chamber	Perforated annular nozzle	5	20	HWA	• Integral time scale • Power density spectra
Hauert et al. (1994)	ISO 1 m^3 chamber	Perforated annular nozzle	5	20	Laser Doppler anemometry (LDA)	• Instantaneous velocities
	12 m^3 silo	N/A	N/A	N/A	LDA	• RMS turbulent velocities
Zhen and Leuckel (1995a, 1995b, 1996)	1 m^3 chamber (L/D=1.2:1)	Perforated hemispheres (35 mm ∅, 15 holes each 5.7 mm ∅)	2 at 5.4 l each	18	HWA	• Instantaneous velocities • RMS turbulent velocities

Van der Wel et al. (1992) used HWA to make turbulence measurements in both the 20 l Siwek and ISO 1 m^3 vessels. The decaying turbulent flow field inside each chamber was sampled at a rate of 50 kHz for a duration of 1.2 s while injecting dust-free air. Although the turbulent flow field had not completely decayed after 1.2 s, the sampling period encompassed ignition delay times for both the 20 l Siwek (60 ms) and ISO 1 m^3 (600 ms) test vessels. By assuming statistically stationary turbulence during a 20 ms time interval, analyses of RMS turbulent velocities, integral time scales and power density spectra were performed. One must question the validity of using 20 ms time windows, since the time from the start of injection to ignition in the 20 l chamber is only 60 ms. As with Pu et al. (1990), the use of HWA also resulted in lack of directional sensitivity. As noted by van der Wel et al. (1992), the power density spectrum presents the intensity and frequency of the turbulent velocity fluctuations of the flow. At an ignition delay time of 600 ms in the 1 m^3 vessel, the power density spectrum was remarkably similar to that in the 20 l sphere at an ignition delay time of 165 ms. However, at the standard ignition delay time of 60 ms, the power density spectra of the 20 l and 1 m^3 vessels were not similar.

Hauert, Vogl, and Radandt (1994) conducted turbulence measurements in a 12 m^3 silo and an ISO 1 m^3 test vessel. Their aim was to compare measurements from an industrial plant with those from a standard 1 m^3 dust explosion test vessel. Furthermore, they attempted to find a relation between the plant-scale and laboratory-scale results, and explore the possibility of conducting 1 m^3 tests under similar conditions of turbulence found in process equipment. In the 1 m^3 vessel, maize starch was injected through the standard perforated annular nozzle at concentrations between 30 and 120 g/m^3. Both horizontal and vertical components of velocity were measured using laser Doppler anemometry (LDA). The measuring location was at the geometric center of the vessel. They presented both instantaneous and RMS turbulent velocities. Since LDA only gives a measurement of velocity when a particle crosses the probe volume (and is successfully validated), the mean and RMS velocities are usually calculated from:

$$\bar{U}=\frac{1}{n}\sum_{i=1}^{n}U_i \tag{2}$$

and

$$U_{\mathrm{RMS}}=\sqrt{\frac{1}{n}\sum_{i=1}^{n}(U_i-\bar{U})^2}=\sqrt{\frac{1}{n}\sum_{i=1}^{n}(U_i')^2}, \tag{3}$$

where $\bar{U}$ is the mean velocity, U_i is the instantaneous velocity of the ith measurement and U_i' is the superimposed fluctuation on the mean of the ith measurement. The use of Eqs. (2) and (3) requires selecting an appropriate number of points (i.e., value of n), normally by choosing an appropriate time window and ensemble averaging. Unfortunately, Hauert et al. (1994) provide no information on their method of data analysis. However, their results claim to show that the pneumatic dispersion process in the 1 m^3 vessel is very time-dependent, with RMS turbulent velocities of both horizontal and vertical velocity components decaying to approximately 1.2 and 5.36 m/s, respectively, after 600 ms (i.e., the standard ignition delay time). It was assumed that the difference between RMS turbulent velocities was due to the arrangement of holes in the perforated annular nozzle. The horizontal and vertical components of the RMS turbulent velocities were found to fit an exponential decay of the form:

$$U_{\mathrm{RMS}}=a\,\mathrm{e}^{-bt}+c, \tag{4}$$

where a, b and c are empirical constants. Hauert et al. (1994) concluded that the RMS turbulent velocities measured in an ISO 1 m^3 vessel were at least 2.5 times larger than those in a pneumatically or mechanically fed 12 m^3 silo. In addition, this conclusion was independent of the method of filling the silo (vertical or tangential feeding), the type of dust, or the dust feed rate.

Zhen and Leuckel (1995a, 1995b, 1996) also measured turbulence parameters during the transient dispersion process. Dispersion tests with both dust-free air and dust-laden air were conducted in a 1 m^3 cylindrical vessel, having a length-to-diameter ratio of 1.2/1. Two air reservoirs (each 5.4 l capacity) were mounted on opposite walls of the vessel. Perforated hemispherical injection nozzles (35 mm in diameter, with 15 holes of 5.7 mm diameter each, giving a total open area of approximately 383 mm^2) were connected to the air reservoirs via two pneumatically operated valves. Instantaneous gas-phase velocities for dust-free air dispersions were measured with HWA at three positions, namely: (1) in the vessel center; (2) 250 mm from the center, along the axis of the two nozzles; and (3) 250 mm from the center, normal to the nozzle axis. As mentioned before, the disadvantage of HWA is its directional insensitivity. Data were recorded at a sampling rate of 20 kHz. An ensemble averaging technique was used to determine the time-dependent mean velocities and RMS turbulent velocities within 2 ms time windows (i.e., 40 data points). Results showed that RMS turbulent velocities increased to approximately 15 m/s at the center of the vessel, then decreased rapidly. The RMS turbulent velocities were found to be considerably higher near the nozzle outlet than further downstream or off the jet axis. After a discharge time of approximately 400 ms, it was observed that the gas-phase flow became more uniform and slightly periodic. The periodic behavior was attributed to a circular flow pattern inside the vessel.

3. Experimental

As previously stated, the key objective of the present study is to characterize the turbulent flow field developed inside the 20 l Siwek chamber during the air dispersion process. To characterize the turbulent flow field, dust-free air was dispersed (i.e., in the absence of a test dust), and a two-channel LDA was used to simultaneously measure horizontal and vertical velocity components. Optical access is extremely limited in the 20 l Siwek chamber. The construction of the 20 l Siwek chamber makes it impossible to use a conventional LDA system. To overcome the problem of limited optical access, a model of the 20 l Siwek chamber was designed and constructed. The model 20 l sphere consists of two hemispherical flanged domes (internal diameter=0.336 m). The flanged domes were constructed by thermoforming a flat sheet of 6.35 mm thick acrylonitrile–butadiene–styrene (ABS) into a wooden hemispherical mold, 0.349 m in diameter. Like the standard Siwek chamber, the model was designed to house the standard outlet valve, a vacuum port to enable partial evacuation of the chamber prior to a test, a pressure transducer port to enable dynamic pressure measurements to be recorded during the air dispersion process, and two 178 mm diameter optical quality glass windows to permit the use of LDA.

A four-beam (two-channel), off-axis forward scatter mode of LDA operation was utilized. The light source was a 4 W, argon-ion laser. A fiber optic transmission and receiving system contained the necessary optics to form the probe volume for particle velocity measurements. The gas-phase flow was seeded with 0.2 μm alumina (Al_2O_3) particles that faithfully follow the gas-phase flow and also exhibit good light scattering abilities. A schematic diagram of the experimental set-up is shown in Fig. 3.

To characterize the flow field inside the model sphere during the air dispersion process, three specific dust dispersion systems were investigated:

1. the deflector plate or rebound nozzle (see Fig. 4), with a total open area of 314 mm^2;
2. the perforated annular nozzle (see Fig. 5), which contains 112 holes, each 3 mm in diameter for a total open area of approximately 791 mm^2; and
3. the "Dahoe" nozzle, which is a wing-type air dispersion nozzle (see Fig. 6) that was recently developed by the group at Delft.

In conducting the LDA measurements, four series of tests were performed:

1. rebound nozzle, positioned parallel to the optical axis of the transmitting lens;
2. rebound nozzle, positioned perpendicular to the optical axis of the transmitting lens;
3. perforated annular nozzle, positioned perpendicular to the optical axis of the transmitting lens; and
4. the "Dahoe" nozzle.

For each nozzle configuration, the measuring volume was positioned at six different locations. Ten repetitive tests were performed at each location. The geometric center of the sphere (location 4) served as the starting point in each series. The model sphere was traversed in 15 mm increments (along the optical axis of the transmitting lens), until 10 repetitive tests were conducted at each of the six measuring locations (3 through 8 inclusive). The geometric center was selected so that LDA measurements were made in the region of ignition during an actual dust explosion test. Approximately 10,000 data points (velocity and time) were collected on each input channel, for each air dispersion test. Two input channels were used, one to capture the horizontal component of the fluid velocity (blue beams at 488 nm) and the other to capture the vertical component of the fluid velocity (green beams at 514.5 nm). In total, over 240 air dispersion tests were performed.

4. Data analysis

Locally weighted regression, or *loess*, is a method of estimating a regression surface through a smoothing procedure by fitting a function of the independent variables locally and in a moving fashion. Macauley (1931) comments that local fitting using polynomials has been used for decades to smooth plots in which the independent variables are equally spaced. Locally weighted regression is an extension of this technique, to more general situations such as randomly spaced independent variables. According to Cleveland and Devlin (1988), the advantage of loess is that local fitting can be used in a much wider class of surfaces without major distortion. Thus, loess is an excellent tool for smoothing a typical instantaneous velocity versus time plot which exhibits excessive scatter, as shown in Fig. 7. By employing loess, the visual information was enhanced by computing and plotting a smooth curve through the data. The gas-phase flow during the pre-ignition period inside the model 20 l sphere is non-stationary; that is, both the mean and fluctuating components of velocity decay with time. In this sense, loess is an exploratory graphical tool, lending insight to the behavior of the non-stationarity of the gas-phase flow.

To conduct locally weighted regression, the user must select a value of f, the parameter used to determine the amount of smoothing. As f increases, the local fit is based on a larger number of points within the neighborhood, and thus the *smoothness* of the fitted curve

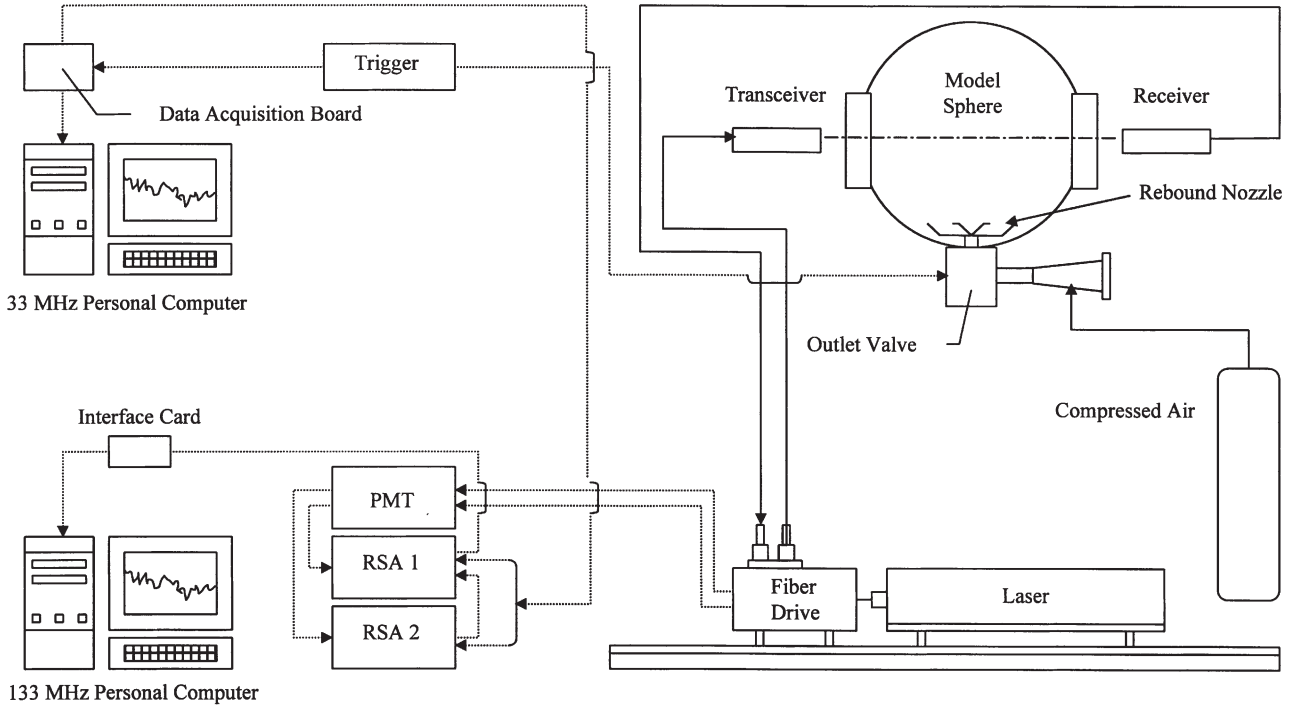

Fig. 3. Schematic diagram of experimental set-up.

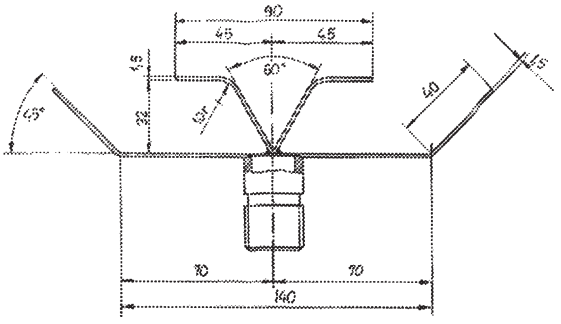

Fig. 4. Rebound nozzle.

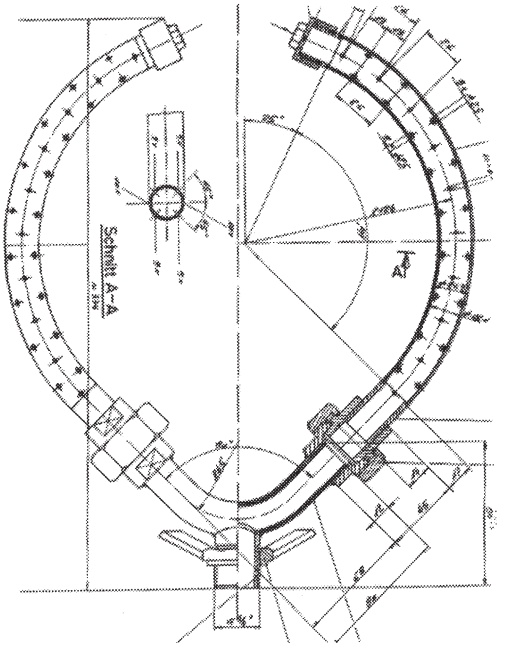

Fig. 5. Perforated annular nozzle.

increases. By applying loess to each of the experimental runs, the intent is to extract the *mean* (which can be visualized as the predominant, or bulk fluid flow) from the instantaneous velocity versus time data. McComb (1996) points out that the number of points within the neighborhood must be large enough to smooth out the turbulent fluctuations but short enough not to average out any imposed time dependence. In addition, Cleveland (1979) states that the goal in the choice of f is to pick a value as large as possible to minimize the variability in the smoothed curve without distorting the pattern of the data. If the smoothed curve is used as a regression surface where the sole purpose of the smoothing is to enhance the visual perception of patterns in the plot, the choice of f is not so critical. In this case one's eyes can partially correct for a less than optimal choice of f. On the other hand, if presented without the underlying (instantaneous velocity versus time) data, more care in choosing f seems warranted. The M plot is a tool to assist in the selection of f in loess. The rationale for this plot is described by Cleveland and Devlin (1988) and is presented in Appendix A, together with an example of an M plot in Fig. A1.

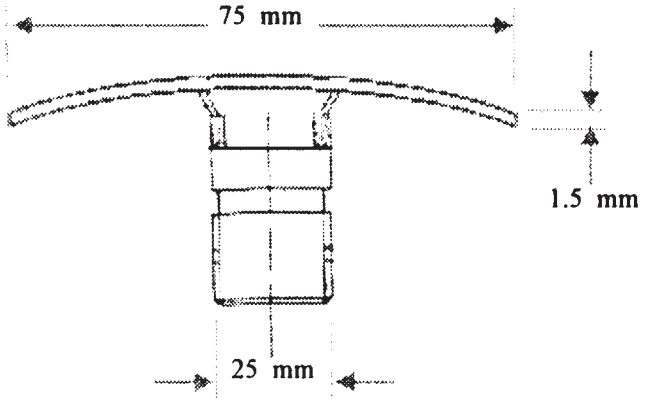

Fig. 6. Dahoe nozzle.

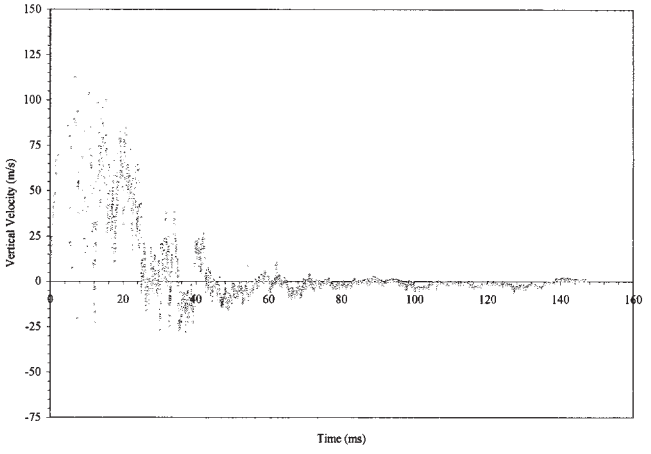

Fig. 7. Instantaneous vertical velocity versus time for one experimental run for the Dahoe nozzle at probe location 5.

5. Discussion of results

We focus initially on results obtained with the "Dahoe" nozzle so as to demonstrate the data analysis and interpretation methodology. Discussion then shifts to the general features of dispersion of dust-free air from all three nozzles and concludes with the influence of dust loading on the gas-phase turbulence. Extensive compilations of data obtained from this work are available elsewhere (Mercer, 1999).

Fig. 7 shows instantaneous vertical velocity plotted against time for one experimental run at probe location 5 (15 mm from the geometric center of the chamber, along the optical axis of the transmitting lens). This plot exhibits a rapidly decaying flow field during the pre-ignition period. Instantaneous vertical velocities range from approximately 100 m/s at 10 ms to approximately 0 m/s by 80 ms. The magnitude of this behavior in the 20 l chamber has been masked in previous studies (Siwek, 1980; Pu et al., 1990) primarily through the use of directional-insensitive HWA. As previously stated, 10 runs were performed at each probe location. The results of 10 overlaid runs are presented in Fig. 8, which also shows a rapidly decaying flow field during the pre-ignition period. This observation is consistent with the work of Pu et al. (1990) performed in a 20 l Siwek chamber, and Hauert et al. (1994) performed in an ISO 1 m^3 vessel. Figs. 7 and 8 show that a significant amount of scatter is present, indicating cycle-to-cycle variations on the vertical component of the gas-phase velocity between successive runs (i.e., air injections).

Furthermore, Figs. 7 and 8 represent a non-stationary flow field, whereby both mean and fluctuating components of the gas-phase velocity decay with time. To analyze this non-stationary signal, the instantaneous velocity can be written as the sum of its mean velocity at a point and a relative motion as a superimposed fluctuation on the mean:

$$U=\bar{U}+U', \tag{5}$$

in which U is the instantaneous velocity in the vertical direction, $\bar{U}$ is the mean vertical velocity, and U' is the superimposed vertical fluctuation on the mean. To extract the mean velocity, loess was applied. The result of applying loess to 10 overlaid runs is shown as the regression line through the data in Fig. 8. This regression curve (i.e., mean flow) decays rapidly with time, from about 50 m/s at 10 ms to ~0 m/s in 80 ms. It can be seen from Eq. (5) that subtracting the mean from the instantaneous velocity will result in superimposed fluctuations on the mean, as shown in Fig. 9. According to Reynolds rules of averaging, if any fluctuating quantity is time-averaged, that average must be zero as a consequence of its definition (McComb, 1996). Thus:

$$\frac{\sum_{i=1}^{n} U_i'}{n}=0. \tag{6}$$

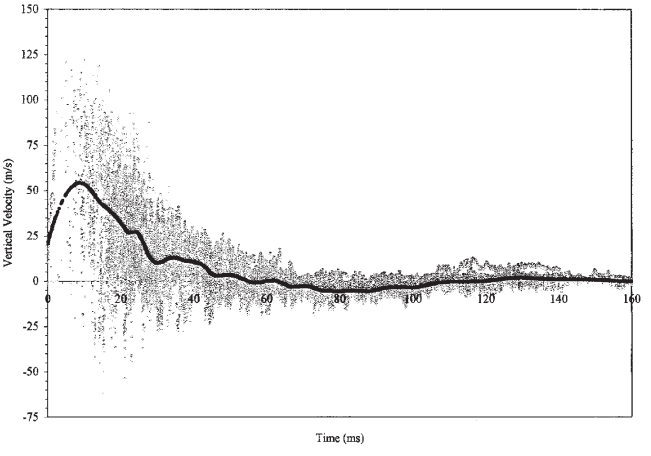

Fig. 8. Instantaneous vertical velocity and the mean flow (loess) versus time for 10 overlaid runs using the Dahoe nozzle at probe location 5.

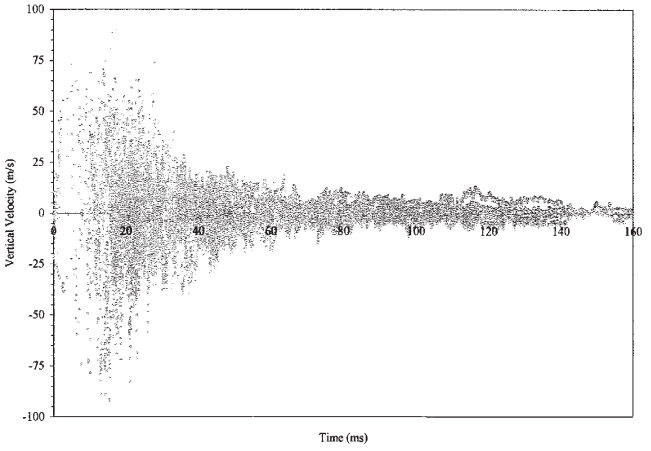

Fig. 9. Superimposed fluctuations on the mean flow versus time for the Dahoe nozzle at probe location 5.

Computation of the average of the superimposed fluctuations on the mean (for the data shown in Fig. 9), using Eq. (6), results in a mean fluctuation of 0.025 m/s over a 120 ms time period (i.e., $n \approx 20{,}000$).

From Eq. (3) it can be seen that when $n=1$, the RMS of the superimposed fluctuations on the mean becomes the absolute value of the superimposed fluctuations on the mean. Thus:

$$\sqrt{\frac{1}{n}\sum_{i=1}^{n}(U_i')^2} = |U_i'| \text{ for } n=1. \tag{7}$$

Fig. 10 shows the absolute value of the superimposed fluctuations on the mean as a function of time. The line is a loess fit of these data, which represents the mean of the absolute value of the superimposed fluctuations on the mean flow. The decaying nature shown in Fig. 10 is consistent with the decaying nature of the RMS determined by ensemble averaging in time windows as in the work of Pu et al. (1990), Hauert et al. (1994) and Zhen and Leuckel (1995a, 1995b, 1996). However, our data show the true extent of the variation in fluctuations.

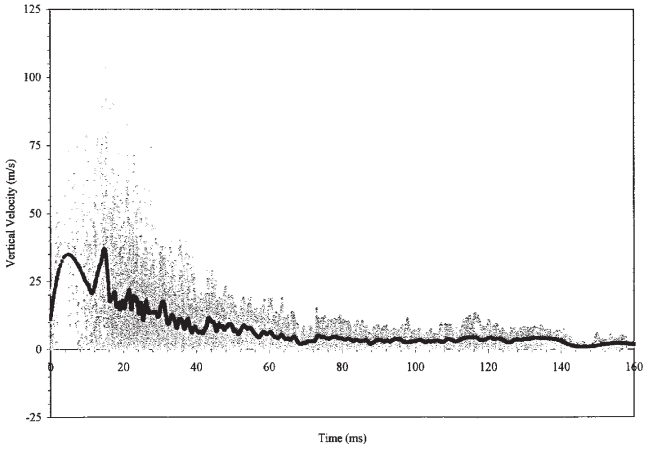

Fig. 10. Absolute values of the superimposed fluctuations on the mean flow and the mean of these (loess) versus time for the Dahoe nozzle at probe location 5.

5.1. Dahoe nozzle

5.1.1. Mean flows

Vertical components of velocity at a delay time of 10 ms across all probe locations indicated predominantly positive (i.e., downward) gas-phase velocities. Due to the nozzle geometry, the gas-phase flow follows the perimeter (i.e., inner wall) of the 20 l chamber. At the top of the spherical chamber, these flows interact and combine to create a large (i.e., about +50 m/s) downward flow in the region of the geometric center at a delay time of 10 ms.

Vertical components of velocity at a delay time of 10 ms generally decreased with increasing probe location, from about +57 m/s (probe location 3) to about +36 m/s (probe location 8). The largest gas-phase velocities occurred in a "central core" (i.e., probe locations 3–5) of the downward-flowing air blast (about +53 m/s). Outside this central core (i.e., probe locations 7 and 8), gas-phase velocities decreased to about +36 m/s.

Horizontal components of velocity at a delay time of 60 ms across all probe locations indicated predominantly negative (i.e., right to left) gas-phase velocities. Predominantly negative gas-phase velocities result from the construction of the outlet valve assembly. The pressurized air storage canister is mounted on the right side of the outlet valve assembly. Upon opening the outlet valve, the air from the storage canister follows the path of least resistance (i.e., shortest entry length) to the partially evacuated vessel. In doing so, the bulk of the air channels to the right inner wall of the outlet valve assembly, thereby exiting the right side of the Dahoe nozzle. Once inside the vessel, the air flows away from the point of entry (i.e., right to left), accounting for the predominantly negative horizontal gas-phase velocities.

Vertical components of velocity at a delay time of 60 ms across all probe locations did not indicate predominant gas-phase velocities in either negative or positive directions. Furthermore, a near-zero mean flow was exhibited at the standard delay time of 60 ms.

5.1.2. Mean of the absolute value of the superimposed fluctuations on the mean flow

Vertical components of absolute values of the superimposed fluctuations on the mean flow (ranging from about 24 to 28 m/s) were larger than horizontal components (ranging from about 16 to 21 m/s) at a delay time of 10 ms. Being independent of direction, these results indicate that larger mean flows exhibit larger superimposed fluctuations. The demarcation between the magnitude of horizontal and vertical superimposed fluctuations on the mean flow is not pronounced at larger delay times

(i.e., 60, 120 and 180 ms) due to the decay of superimposed fluctuations on the mean flow once the injection of dispersing air stops.

5.2. Perforated annular nozzle

5.2.1. Mean flows

Horizontal and vertical components of velocity did not reveal predominant gas-phase velocities at probe locations 3 through 8 at 10, 60, 120 or 180 ms. The non-predominant flow patterns, as evidenced by the chaotic nature of gas-phase velocities, is attributed to both the circular geometry of the perforated annular nozzle and to the uniformity of dispersion holes drilled around the nozzle.

5.2.2. Mean of the absolute value of the superimposed fluctuations on the mean flow

There was no clear demarcation between horizontal and vertical components of velocity of superimposed fluctuations on the mean flow at 10, 60, 120 and 180 ms.

5.3. Rebound nozzle positioned parallel with the optical axis

5.3.1. Mean flows

Horizontal components of velocity at a delay time of 10 ms across all probe locations indicated predominantly negative (i.e., right to left) gas-phase velocities. These predominantly negative horizontal gas-phase velocities were consistent with those observed using the Dahoe nozzle and occur due to the construction of the outlet valve assembly.

Vertical components of velocity at a delay time of 10 ms across probe locations 3–7 indicated predominantly positive (i.e., downward) gas-phase velocities. As with the Dahoe nozzle, the airflow follows the perimeter of the 20 l chamber and interacts at the top, combining to create a predominant downward flow in the region of the geometric center at a delay time of 10 ms.

5.3.2. Mean of the absolute value of the superimposed fluctuations on the mean flow

Vertical components of absolute values of the superimposed fluctuations on the mean flow across all probe locations were larger than horizontal components at a delay time of 10 ms. This again indicates that larger mean flows exhibit larger superimposed fluctuations. This demarcation between the magnitude of horizontal and vertical superimposed fluctuations on the mean flow supports the assertion of predominant gas-phase flow patterns in the vertical direction.

5.4. Rebound nozzle positioned perpendicular with the optical axis

5.4.1. Mean flows

Horizontal components of velocity at a delay time of 10 ms across all probe locations indicated predominantly negative (i.e., right to left) gas-phase velocities. These were consistent with those observed using the Dahoe nozzle and the rebound nozzle positioned parallel with the optical axis.

Vertical components of velocity at a delay time of 10 ms across all probe locations indicated predominantly positive (i.e., downward) gas-phase velocities. Again, similar to results obtained using both the Dahoe nozzle and the rebound nozzle positioned parallel with the optical axis, the air flow follows the perimeter of the 20 l chamber. Likewise, these flows interact and combine to create a large (i.e., about +45 m/s at probe locations 3 through 8) downward flow in the region of the geometric center at a delay time of 10 ms.

Vertical components of velocity at a delay time of 60 ms across all probe locations indicated predominantly negative (i.e., upward) gas-phase velocities. A possible explanation for these negative velocities is a reflected shock (i.e., reflected gas-phase elements) traveling upwards from the bottom hemisphere of the 20 l chamber. Interestingly, vertical components of velocity at a delay time of 60 ms across probe locations 3, 4, 5, 6 and 8 for the rebound nozzle positioned parallel with the optical axis also indicated predominantly negative (i.e., upward) gas-phase velocities. A reflected shock traveling upwards from the bottom hemisphere of the chamber would be independent of nozzle rotation since the chamber is symmetric about the vertical axis.

5.4.2. Mean of the absolute value of the superimposed fluctuations on the mean flow

Vertical components of absolute values of the superimposed fluctuations on the mean flow were larger than horizontal components at a delay time of 10 ms. This again indicates that larger mean flows exhibit larger superimposed fluctuations. Similar to results generated with the rebound nozzle positioned parallel with the optical axis, the magnitude of vertical superimposed fluctuations on the mean flow was larger than horizontal superimposed fluctuations on the mean flow at a delay time of 10 ms. This supports the assertion of predominant gas-phase flow patterns in the vertical direction.

5.5. Influence of dust loading on gas-phase turbulence

The 20 l sphere at a pressure of 1 bar contains about 21 g of air, whereas the typical mass loading of dust ranges from 2.5 to 20 g (nominal dust concentrations of 125 g/m^3 to 1000 g/m^3). The issue, therefore, is whether

the decay of turbulence of a dust cloud will deviate significantly from that of dust-free air.

Zhen and Leuckel (1995a, 1995b, 1996) conducted an experimental investigation of the generation of dust clouds through air discharging from pressure reservoirs. Their experiments were conducted in a 1 m^3 cylindrical vessel with two 5.4 l dust reservoirs (see Table 2). Tests were done with different mass loadings of cornstarch. Pressure–time histories were measured at the nozzle inlets and within the air reservoirs.

They found that the discharge process was strongly affected by the dust loading and initial reservoir air pressure. Results for 250 g dust loading in each reservoir (500 g/m^3) and a reservoir pressure of 18 bar indicated a total discharge time of 450 ms. However, concentration measurements indicated that all of the dust was discharged in 150 ms. This implied a two-stage process: first, discharge of the dust/air mixture (≈150 ms) followed by discharge of dust-free air (≈300 ms), which created additional turbulence in the dust/air suspension.

HWA was used to measure flow velocities and turbulence intensity for dust-free air injections. Using the measured pressure–time histories and a model based on turbulent free jet flows they developed an "equivalent jet" concept in which:

$$u_{eq}=\frac{\dot{M}}{\dot{m}} \quad \text{and} \quad d_{eq}=\frac{2\dot{m}}{\sqrt{\pi\rho\dot{M}}}. \tag{8}$$

Here u_{eq} and d_{eq} are the equivalent jet outlet velocity and diameter, in which $\dot{M}$ and $\dot{m}$ are the outlet momentum flux and outlet mass flow rate and ρ is the density of the mixture in the vessel. In this manner they correlated the turbulence intensity measured in dust-free air with that estimated for dust-laden air, and found that the intensity of dust-dispersion-induced turbulence was higher than for dust-free air. Hence, they concluded that turbulence measurements in dust-free air underestimate turbulence intensities in dust-laden air and need to be corrected using u_{eq} and d_{eq} (which need to be estimated from pressure–time histories).

De Heij (1998) conducted a series of dust injections in the model 20 l sphere using cornstarch dispersed with nitrogen (for safety reasons). To enable turbulence measurements to be made with the LDA, dust mass loading ≤12.5 g (nominal dust concentration of 625 g/m^3) had to be used. Each cornstarch injection was preceded by a seeded dust-free air injection so as to measure the gas-phase fluctuations. The results are presented in Fig. 11. The thick line shows the decay of the RMS of the vertical velocity fluctuations generated by a single injection of dust-free air. The thin lines indicate the deviation from the thick line when different mass loadings of cornstarch were injected. Aside from the considerable scatter with the cornstarch injections, the results indicate that

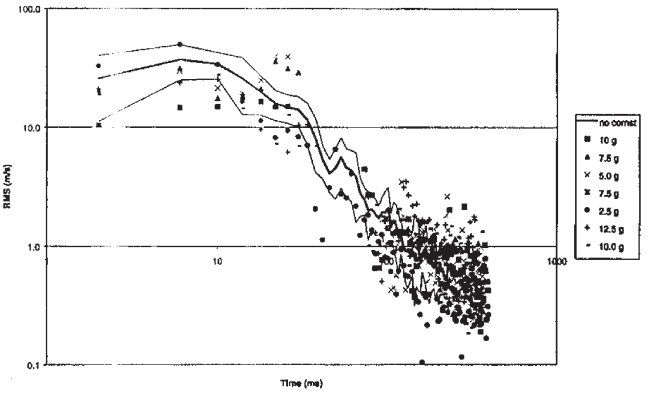

Fig. 11. Root-mean-square values of the vertical velocity component measured at the geometric center of the 20 l chamber using the rebound nozzle perpendicular to the optical axis of the LDA after injecting cornstarch dust. From de Heij (1998).

the turbulent fluctuations of the gas-phase behave more or less independently of the presence of the dust.

The work of Zhen and Leuckel (1995a, 1995b, 1996) appears to be at variance with the work of de Heij (1998). However, Zhen and Leuckel's measurements were made in dust-free air with a direction-insensitive HWA whereas de Heij's were made in the presence of dust-laden air using LDA. It is clear that further work is needed to adequately resolve the issue.

6. Conclusions

An experimental investigation has been undertaken to characterize the turbulent flow field developed inside the 20 l Siwek chamber during the dust-free air dispersion process. An ABS model of the 20 l Siwek chamber has been designed and constructed with optical quality windows enabling LDA to be used for the measurement of turbulence. Three specific dust dispersion systems were investigated: (1) the deflector plate (rebound nozzle); (2) the perforated annular nozzle; and (3) the "Dahoe" nozzle. Locally weighted regression, or *loess*, was used as a method of estimating a regression surface through a smoothing procedure by fitting a function of the independent variables locally and in a moving fashion. To implement locally weighted regression, the M plot was used as a tool for assisting in the selection of the smoothing parameter (*f*). From these results, the following conclusions are drawn.

- Due to geometries of both the Dahoe and rebound nozzles, the bulk gas-phase flow (i.e., mean flow) developed by both nozzles follows the perimeter (i.e., inner wall) of the model 20 l chamber. At the top of the spherical chamber, these flows interact and combine to create a predominant downward flow in the

region of the geometric center early (i.e., ≈10 ms) in the air dispersion process.

- Horizontal components of velocity from the Dahoe nozzle at the standard delay time of 60 ms indicated predominantly negative (i.e., right to left) gas-phase velocities. These predominantly negative velocities resulted from the construction of the outlet valve assembly, which allowed air to "channel" through the valve.
- Horizontal components of velocity from the rebound nozzle in both parallel and perpendicular configurations at a delay time of 10 ms also indicated predominantly negative (i.e., right to left) gas-phase velocities. Similar to results from the Dahoe nozzle, these predominantly negative gas-phase velocities resulted from the construction of the outlet valve assembly.
- Predominantly negative gas-phase velocities in the horizontal direction due to "channeling" were not observed using the perforated annular nozzle. This was due to the circular geometry of the perforated annular nozzle as well as the uniformity of dispersion holes around the nozzle.
- Both horizontal and vertical components of velocity from the perforated annular nozzle did not reveal predominant gas-phase velocities at probe locations 3 through 8 inclusive at 10, 60, 120, or 180 ms. The chaotic nature of these flows is attributed to the circular geometry of the perforated annular nozzle as well as the uniformity of dispersion holes around the nozzle.
- Vertical components of velocity at the standard delay time of 60 ms across all probe locations using the rebound nozzle (in both parallel and perpendicular configurations) indicated predominantly negative gas-phase velocities. A pressure pulse reflected from the bottom hemisphere of the 20 l chamber was believed to be responsible for these results.
- Vertical components of the mean of the absolute value of the superimposed fluctuations on the mean flow for both Dahoe and rebound nozzles were larger than horizontal components early (i.e., ≈10 ms) in the air dispersion process. These results indicate that larger mean flows exhibit larger superimposed fluctuations. As well, the demarcation between the magnitudes of vertical and horizontal superimposed fluctuations on the mean flow is not pronounced at larger (i.e., at 60, 120 and 180 ms) delay times due to the decay of superimposed fluctuations once the injection of dispersing air stops.
- Results of the mean of the absolute value of the superimposed fluctuations on the mean flow from the perforated annular nozzle indicated no clear demarcation between magnitudes of horizontal and vertical components of superimposed fluctuations at 10, 60, 120 and 180 ms. These results are consistent with the chaotic nature of gas-phase flows developed by the perforated annular nozzle.

Acknowledgements

The group from Canada gratefully acknowledges financial assistance from the Natural Sciences and Engineering Research Council of Canada.

Appendix A. Details of the M plot

The M plot is a tool for assisting in the selection of f in locally weighted regression. Suppose $\hat{g}_f(x_i)$ is the local regression estimate for a particular value of f, then the expected mean-squared-error summed over the x_i in the sample and divided by σ^2 is defined as:

$$M_f = \frac{E\sum_{i=1}^{n}(\hat{g}_f(x_i)-g(x_i))^2}{\sigma^2}, \tag{A1}$$

where $\hat{g}_f(x_i)$ is the local regression estimate for a particular value of f, $g(x_i)$ is the *true* dependent variable at x_i, $(\hat{g}_f(x_i)-g(x_i))$ is the residual value at x_i, and σ^2 is the *true* variance around $\hat{g}_f(x_i)$. Let us suppose that $\hat{\sigma}_s^2$ is an estimate of the true variance (σ^2), as a result of smoothing. The subscript s refers to the span, where f is small, depending on the nature of the data in the plot. This way (with a small value of f), $\hat{g}_s(x_i)$ (that is, the fitted values) will closely follow the *trend* of the data and bias will be negligible, which results in an unbiased estimate of the true variance (σ^2). It should be noted that σ^2=(standard deviation)^2=variance, where the standard deviation is a measure of how widely values are dispersed from the mean. Via a statistical derivation (see Cleveland & Devlin, 1988), M_f can be estimated with $\hat{M}_f$, where:

$$\hat{M}_f = \hat{B}_f + V_f \tag{A2}$$

and $\hat{B}_f$ is the contribution of bias to $\hat{M}_f$ (the estimated mean-squared-error), and V_f is the contribution of variance. That is:

$$\hat{B}_f = \hat{\varepsilon}_f'\hat{\varepsilon}_f/\hat{\sigma}_s^2 - \mathrm{tr}(I-L_f)'(I-L_f) \tag{A3}$$

and

$$V_f = \mathrm{tr}\, L_f'L_f, \tag{A4}$$

where $\hat{\varepsilon}_f$ is the residual between the *true* dependent variable and the local regression estimate for a particular value of f, tr is the trace of a matrix (that is, the sum of the diagonal elements), I is an $n\times n$ identity matrix, and L_f is an $n\times n$ matrix resulting from locally weighted regression, applied at a particular value of f. If, for a

particular value of the span, $\hat{g}_f(x_i)$ are a nearly unbiased estimate (that is, the contribution of bias to the estimated mean-squared-error is negligible), the expected value of $\hat{B}_f \approx 0$. Then, the expected value of $\hat{M}_f \approx V_f$ from Eq. (A2). As f increases, bias is introduced, $\hat{B}_f$ then has a positive expected value and then the expected value of $\hat{M}_f$ exceeds V_f. V_f is defined as the equivalent number of parameters of the fit, which is a measure of the amount of smoothing done by locally weighted regression. V_f decreases as f increases, so more smoothing results in a lower equivalent number of parameters.

The M plot is a graph of $\hat{M}_f$ (the estimated mean-squared-error) versus V_f (the equivalent number of parameters) for a selection of f values. This allows an observation of the trade-off between the contributions of bias and variance to the mean-squared-error as f changes. With respect to Fig. A1, the filled circles show estimates of the mean-squared-error ($\hat{M}_f$ values) at various values of f ranging from 0.35 (rightmost circle) to 1.0 (leftmost circle). $\hat{M}_f$ values are plotted against their expected values under an assumption of no bias, that is $\hat{M}_f = V_f$, which is the $y=x$ line. The vertical distance between the filled circles and the $y=x$ line is the contribution of bias to the estimate of the mean-squared-error. The ends of the vertical lines show 90% intervals and the tick marks show 80% intervals of the distribution of the estimates of the mean-squared-error under an assumption of no bias; therefore, these are an indication of the contribution of variance to the estimated mean-squared-error. The vertical lines are also helpful for judging variation — that is, to show information about the distribution of $\hat{M}_f$ when there is no bias. As a rule of thumb, Cleveland (1979) recommended f values should be chosen in the vicinity of the estimate of the mean-squared-error (filled circles) contacting the upper 80% interval of the distribution of the estimates of the mean-squared-error under an assumption of no bias. Using this approach with respect to Fig. A1, f was chosen as 0.75, corresponding to approximately 4.5 equivalent parameters.

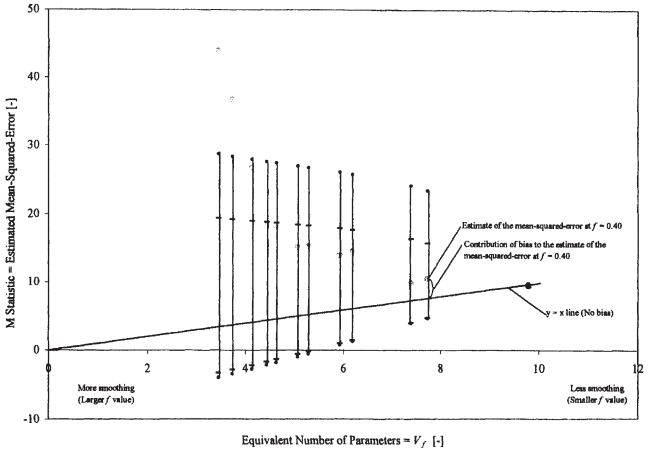

Fig. A1. M plot.

References

Abbott, J. A. (1985). *BMHB survey of dust fire and explosions in the UK 1979–84*. British Materials Handling Board.

ASTM E1226-94 (1994). Standard test method for pressure and rate of pressure rise for combustible dusts. In *Annual book of ASTM standards* (Vol. 14.02). Philadelphia, PA: American Society for Testing and Materials.

Bartknecht, W. (1989). *Dust explosions, course, prevention, protection.* Berlin: Springer-Verlag.

Bradshaw, P. (1971). *An introduction to turbulence and its measurement.* Oxford: Pergamon Press.

Cleveland, W. S. (1979). Robust locally weighted regression and smoothing scatterplots. *Journal of the American Statistical Association*, *74* (368), 829–836.

Cleveland, W. S., & Devlin, S. J. (1988). Locally weighted regression: an approach to regression analysis by local fitting. *Journal of the American Statistical Association*, *83* (403), 596–610.

de Heij, W. B. C. (1998). On the application of lase doppler anemometry to the transient flow inside the standard 20-litre explosion sphere. *Master's thesis*. Delft, The Netherlands: Delft University of Technology.

Hauert, F., Vogl, A., & Radandt, S. (1994). Measurement of turbulence and dust concentration in silos and vessels. In *Proceedings of the 6th International Colloquium on Dust Explosions, Shenyang, PRC*.

ISO 6184/1 (1985). Explosion protection systems — part 1: Determination of explosion indices of combustible dusts in air. International Standards Organization.

Jeske, A., & Beck, H. (1989). Evaluations of dust explosions in the Federal Republic of Germany. *EuropEx Newsletter*, *9* (July), 2–4.

Kauffman, C. W., Mestrich, K. R., Regan, R. P., & Seymour, T. H. (1996). Dust explosions in the US grain industry — the effects of research, regulations, and education. In *Proceedings of the Seventh International Colloquium on Dust Explosions, International Symposium on Hazards, Prevention and Mitigation of Industrial Explosions, Bergen, Norway* (pp. 1.1–1.14).

Lunn, G. (1992). *Guide to dust explosion prevention and protection, part 1 — venting* (2nd ed.). Rugby, UK: Institution of Chemical Engineers.

Macauley, F. R. (1931). *The smoothing of time series.* New York: National Bureau of Economic Research.

McComb, W. D. (1996). *The physics of fluid turbulence.* Oxford: Oxford Science Publications.

Mercer, D. B. (1999). An investigation of turbulence in a standard dust explosion test vessel. *M.A.Sc. thesis*. Halifax, Canada: Dalhousie University.

Porter, B. (1989). Industrial incidents. Paper presented at Dust Explosions: Assessment, Prevention and Protection, London, 24th November.

Pu, Y. K., Jarosinski, J., Johnson, V. G., & Kauffman, C. W. (1990). Turbulence effects on dust explosions in the 20-L spherical vessel. In *Proceedings of 23rd International Symposium on Combustion* (pp. 843–849). Pittsburgh, PA: The Combustion Institute.

Siwek, R. (1980). Experimental methods for the determination of explosion characteristics of combustible dusts. In *Proceedings of 3rd International Symposium on Loss Prevention and Safety Promotion in the Process Industries, Basel, Switzerland, Vol. 3*. (pp. 839–850).

van der Wel, P. G. J., van Veen, J. P. W., Lemkowitz, S. M., Scarlett, B., & van Wingerden, C. J. M. (1992). An interpretation of dust explosion phenomena on the basis of time scales. *Powder Technology*, *71*, 207–215.

Zhen, G., & Leuckel, W. (1995a). The dynamic flow condition of dust dispersion induced turbulence. In *Proceedings of the 10th Symposium on Turbulent Shear Flows, The Pennsylvania State University, Pittsburgh, PA* (pp. 25–27).

Zhen, G., & Leuckel, W. (1995b). Influence of transient injection

induced turbulent flow on gas and dust explosions in a closed-vessel. In J. J. Mewis, H. J. Pasman, & E. E. De Rademaker, *Loss and Safety Promotion in the Process Industries, Proceedings of the 8th International Symposium, Antwerp, Belgium* (pp. 257). Amsterdam: Elsevier.

Zhen, G., & Leuckel, W. (1996). Determination of dust–dispersion induced turbulence and its influence on dust explosions. *Combustion Science and Technology*, *113-114*, 629–639.